Operational modes of a ferroelectric LCoS modulator for displaying binary polarization, amplitude, and phase diffraction gratings

Antonio Martínez-García,[1] Ignacio Moreno,[1,*] María M. Sánchez-López,[2] and Pascuala García-Martínez[3]

[1]Departamento de Ciencia de Materiales, Óptica y Tecnología Electrónica, Universidad Miguel Hernández, 03202 Elche, Spain

[2]Instituto de Bioingeniería and Departamento de Física y Arquitectura de Computadores, Universidad Miguel Hernández, 03202 Elche, Spain

[3]Departamento de Óptica, Universitat de València, 46100 Burjassot, Spain

*Corresponding author: i.moreno@umh.es

Received 18 February 2009; revised 2 April 2009; accepted 28 April 2009; posted 29 April 2009 (Doc. ID 107704); published 15 May 2009

We analyze the performance of a ferroelectric liquid crystal on silicon display (FLCoS) as a binary polarization diffraction grating. We analyze the correspondence between the two polarization states emerging from the displayed grating and the polarization and intensity of the diffracted orders generated at the Fourier diffraction plane. This polarization-diffraction analysis leads, in a simple manner, to configurations yielding binary amplitude or binary phase modulation by incorporating an analyzer on the reflected beam. Based on this analysis, we present two useful variations of the polarization configuration. The first is a simplification using a single polarizer, which provides equivalent results for amplitude or phase modulation as the more general operational mode involving two polarizers. The second variation is proposed to compensate the reduction of the diffraction efficiency when the operating wavelength differs from the design one (for which the FLCoS liquid-crystal layer acts as a half-wave plate). In this situation we show how the ideal grating performance can be recovered in spite of the phase-shift mismatch originated by chromatic dispersion. In all cases, we provide experimental results that verify the theoretical analyses.

OCIS codes: 230.3720, 050.0050, 230.0230.

1. Introduction

Liquid-crystal displays (LCDs) have become attractive devices for applications such as diffractive optics, adaptive optics, or optical metrology [1,2]. While nematic LCDs are the dominant technology, devices based on ferroelectric liquid crystals have grown in importance since they can switch up to 100 times faster than standard nematic liquid crystals. Ferroelectric LCDs (FLCDs) have found applications in diffractive optics for the generation of digital holograms [3,4], adaptive beam steering systems [5], and polarization gratings [6–8]. Recently, liquid-crystal on silicon (LCoS) technology is becoming particularly attractive for use as spatial light modulators (SLMs) because of its high reflectivity and excellent fill factor, and ferroelectric LCoS (FLCoS) displays have been also developed for that purpose. These are reflective devices suitable for applications when a fast optical response is required [9–11].

The ferroelectric liquid-crystal layer inside a FLCoS device can be considered as a uniaxial medium with the optical axis in the layer plane (the optical axis is given by the direction of the liquid-crystal director). The device acts as a rotatable waveplate,

0003-6935/09/152903-12$15.00/0

such that the direction of the applied voltage rotates the birefringent axes by an angle $\Delta\theta$ between two stable positions [12]. A common FLC modulator configuration for display applications consists of adjusting the FLC layer to act as a half-wave plate (HWP) (introducing a phase shift $\phi = 180°$) with a switching angle (also named tilt angle) of $\Delta\theta = 45°$ [1]. In this ideal situation, input of linearly polarized light incident onto the display results in two emerging polarization states that remain linear and are mutually orthogonal [12]. Therefore, if the output polarizer is oriented parallel to one of these linear states, this state is fully transmitted, while the second one is fully absorbed. However, when any of these ideal conditions is not accomplished (typically the phase shift differs from the value $\phi = 180°$ when the operating wavelength is not the design one) the two emerging states do not remain orthogonal, and the ideal performance as an intensity optical switch with maximum contrast ratio is lost. Strategies to compensate this effect and recover an almost perfect performance have been accomplished by using elliptically polarized light [12,13].

Here we analyze the performance of a FLCoS display to generate a polarization diffraction grating (PDG). PDGs are diffraction gratings with a periodic spatial variation of the state of polarization (instead of the periodic variation of a scalar magnitude as in standard amplitude or phase diffraction gratings) [14]. The PDG period is high enough compared to the incident light wavelength, so the scalar diffraction treatment can be applied to each orthogonal polarization components separately. Different PDG designs have been proposed in the literature [15–17], demonstrating novel and interesting diffraction properties, as well as applications for polarimetry. Since FLCDs are binary devices, we will consider here only binary PDG. In fact, some of the early works on PDG were developed using FLCDs [6,8]. The novelties of our approach with respect to these previous works are: (1) We use a recently developed combined Jones matrix–Fourier transform approach that was introduced to analyze polarization-diffraction elements [18], which provides an alternative, complementary, and powerful method to analyze PDG. (2) We present how this PDG analysis leads, in a simple and direct way, to polarization configurations leading to their actuation as either binary amplitude or as a binary phase diffraction grating. (3) Finally, we show how the reduction of the PDG efficiency caused by the phase-shift mismatch can be compensated by illuminating the display with elliptically polarized light.

The outline of the paper is the following. In Section 2 we briefly review and apply a reverse engineering method to characterize the FLC modulator physical parameters required to properly operate the display. As a result, we experimentally characterize the rotation of the principal axes of our FLCoS display, as well as the phase-shift introduced for two different operating wavelengths. We show that, for one of the wavelengths, the display operates in the ideal mode, while there is an important phase mismatch for the second wavelength. In Section 3 we present the theoretical study of the binary PDG based on the application of the Jones–Fourier formalism [18]. We derive the intensity and polarization properties of the diffraction orders generated by a grating addressed to the display. This analysis is then applied in Section 4 to the simplest case of a binary HWP PDG to derive the configurations leading to amplitude or phase diffraction gratings. In Section 5 this analysis is extended to the case when the wavelength is not the design one, and a method to optimize the diffraction efficiency based on using an elliptically polarized light configuration is presented. In all cases, we include experimental results that verify these theoretical studies. Finally, the conclusions of the work are provided in Section 6.

2. Characterization of the FLCoS Physical Parameters

One first step when using a commercial LCD for nondisplay applications is the characterization of the physical parameters that control the optical modulation of the device. This knowledge allows adapting different polarization configurations to produce different responses. In our case, we use a commercial FLCoS display from CRL-Opto, model RXGA 1.5C. This is a reflective display with 1024×768 pixels, each with an active area of $11.4\,\mu\text{m} \times 11.4\,\mu\text{m}$ and a pixel pitch of $12\,\mu\text{m} \times 12\,\mu\text{m}$ (thus having an excellent fill factor of more than 90%). This LCD is designed to display color images by using the field sequential color (FSC) technique. For that reason, the device is integrated with a white LED that sequentially illuminates the display with red, green, and blue light. This sequential red–green–blue (RGB) illumination is synchronized with RGB color image components that are displayed in the device. The device is also designed to produce grayscale levels by using pulse width modulation (PWM), achieving 12 bits of color depth (4 bits for each channel).

In our case, and since we are interested in its use as a diffraction grating, we substitute the white LED sequential illumination by a continuous monochromatic illumination from an Ar—Kr laser. Figure 1(a) shows our experimental setup. The FLCoS modulator is illuminated with the unexpanded Ar—Kr laser, and polarizer P_1 selects the orientation of the input polarization. An interference filter (IF) is used to select the wavelength of the laser (568 or 647 nm). An achromatic quarter-wave plate (QWP) is used to generate circularly-polarized light before P_1 to maintain constant intensity impinging on the display as polarizer P_1 is rotated. To avoid the use of beam splitters, we illuminate the display with a small angle of incidence of only 1.5°. The reflected beam is directed onto a second polarizer (P_2) and to an optical detector (Newport model 1815-C). The detected signal is monitored on an oscilloscope.

The physical parameters that determine the device's optical modulation are the liquid crystal (LC)

director orientation and its angular rotation ($\Delta\theta$), induced upon applying a voltage signal, and the phase shift (ϕ), introduced by the LC layer for the operating wavelength. Here we apply a simple reverse engineering procedure proposed in [12] to measure these physical parameters. The method consists of simultaneously rotating both polarizers (P_1 and P_2), while keeping them always crossed, and measuring the transmitted intensity. The normalized intensity of the reflected beam in this situation is given by [7]

$$i = \sin^2(2\varphi)\sin^2\left(\frac{\phi}{2}\right), \qquad (1)$$

where $\varphi = \theta_{P1} - \theta_F$ represents the relative angle between the input polarizer (oriented at θ_{P1}) relative to the FLC director (oriented at θ_F), and ϕ is the phase shift introduced by the LC layer.

When the device is switched on, a bipolar electrical signal with zero mean value is addressed to each pixel, resulting in two stable LC director orientations (θ_{Fa} and θ_{Fb}), each one corresponding to a sign inversion of the electrical signal. Figure 1(b) shows an example of the oscilloscope trace measurement for an arbitrary orientation of the polarizers (here the input and output polarizers were both oriented at 15°). In this result, a uniform white screen has been addressed to the display to provide equal signal to all the pixels of the LCD. The selected laser wavelength is $\lambda = 568$ nm. Two intensity levels (i_a and i_b) are clearly visible, corresponding to the two LC stable orientations (θ_{Fa} and θ_{Fb}). In addition, narrow peaks appear at the polarity transitions of the voltage signal. If a black uniform image (instead of the former white uniform image) is addressed to the display, an inversion of the intensity signal is obtained for the same configuration [see Fig. 1(c)]. The usual display application is based on synchronizing this intensity transmission signal with the illumination sequence.

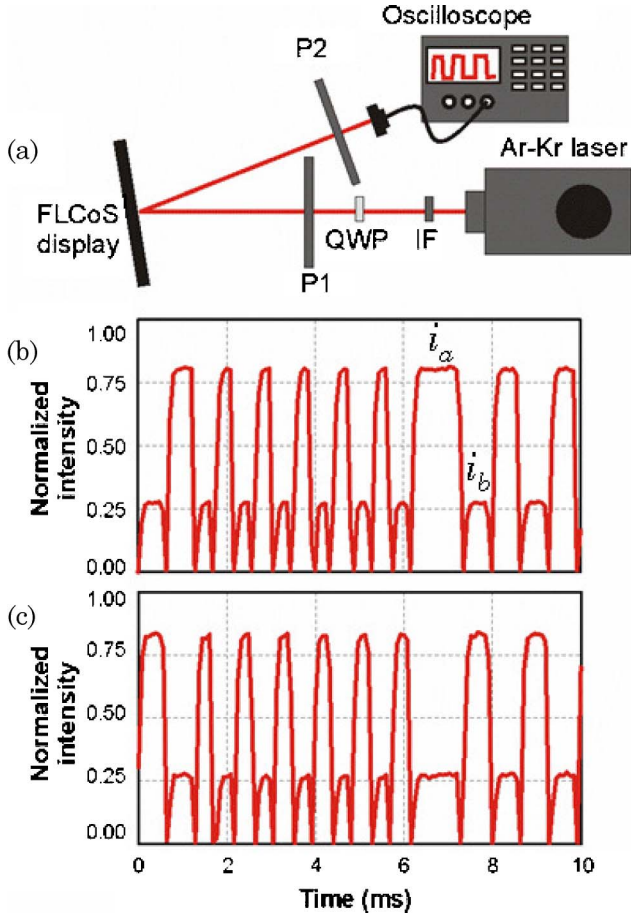

Fig. 1. (Color online) (a) Scheme of the operating system. (b), (c) Oscilloscope traces corresponding to the detected optical intensity for $\lambda = 568$ nm with the two polarizers oriented at 15°. (b) FLCoS displays a uniform white screen. (c) FLCoS displays a uniform black screen.

Following the characterization procedure in [12], intensities i_a and i_b are measured when polarizers P_1 and P_2 are crossed and simultaneously rotated. Figure 2 shows the experimental results of the normalized intensity detected for the two Ar—Kr laser lines of 568 and 647 nm, respectively. The input polarizer θ_{P1} is rotated in the range [0°–180°] and, for each orientation, the second polarizer (analyzer) is always crossed $\theta_{P2} = \theta_{P1} + 90°$. The harmonic function in Eq. (1) is experimentally observed in Fig. 2. Null intensity is obtained for both wavelengths at $\theta_{P1} = 0°$ and $\theta_{P1} = 90°$ for the second level (intensity i_b), and at $\theta_{P1} = 45°$ and $\theta_{P1} = 135°$ for the first level (intensity i_a). These angles denote the orientations of the neutral axes of the FLC wave-plate layer in the two stable positions, and therefore we experimentally verify a tilt angle rotation $\Delta\theta_F = 45°$ between them. According to Eq. (1), maximum relative transmittance equal to $\sin^2(\phi/2)$ is obtained between two null minima. For $\lambda = 568$ nm, the maximum transmission reaches practically 100% transmission indicating a phase shift close to the ideal value of $\phi = 180°$ (HWP behavior). On the contrary, for $\lambda = 647$ nm, the maximum transmission reaches a value around 63%, indicating a phase shift of only $\phi = 105°$.

Once the physical parameters of the display have been calibrated, the polarization configuration can be properly adjusted. A white screen is addressed

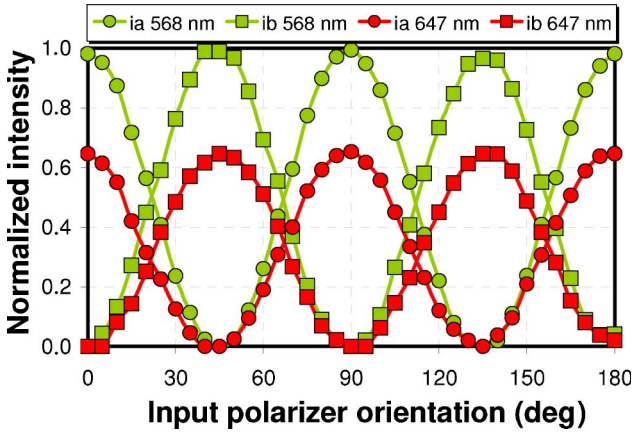

Fig. 2. (Color online) Normalized transmittances i_a and i_b of the system polarizer–FLCoS display–analyzer, as a function of the input polarizer angle. The analyzer is always crossed to the input polarizer. Two Ar—Kr laser wavelengths are used: $\lambda = 568$ nm and $\lambda = 647$ nm, respectively.

once again to the display, and the wavelength $\lambda = 568\,\text{nm}$ providing the ideal phase shift is selected. The input polarizer is oriented at $\theta_{P1} = 0°$, parallel to the first stable LC director orientation. The output state will emerge linearly polarized at 0° for the first stable LC orientation, since the input polarization coincides with the principal axis. On the contrary, light will emerge linearly polarized at 90° for the second LC stable orientation (where the axes have rotated by $\Delta\theta = 45°$). Figure 3 shows the oscilloscope traces corresponding to different orientations of the analyzer when a uniform white image is addressed to the display. In Fig. 3(a) the analyzer is oriented parallel to the polarizer ($\theta_{P2} = 0°$). For this configuration we observe a perfect intensity rectangular response. As expected, when the analyzer is rotated by 90° [Fig. 3(c)] the inversion of the previous intensity signal is observed. When the analyzer is oriented at 45° or 135°, the analyzer angle bisects the two linear states emerging from the modulator, and both states transmit with the same relative intensity of 0.5. Figures 3(b) and 3(d) show this effect. However, the transitions between the two stable states are clearly visible as narrow peaks that point up or down depending on the analyzer orientation. These peaks arise from the rotation of the LC molecules between the two stable orientations, as was noted in [12]. Next, we show the direct correspondence between the modulation responses in Fig. 3 and the different actuations of the display as a one-dimensional diffraction grating with black and white addressed gray levels.

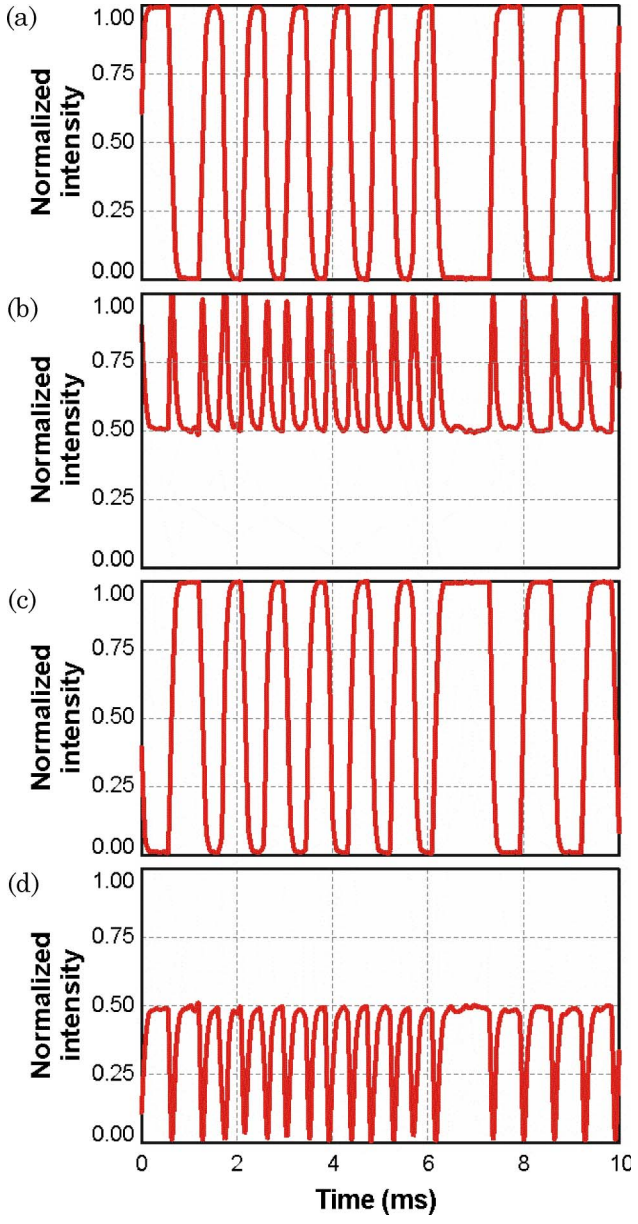

Fig. 3. (Color online) Oscilloscope traces corresponding to the detected optical intensity for $\lambda = 568\,\text{nm}$, when the FLCoS displays a white uniform screen and with the input polarizer oriented at 0°. The output polarizer is oriented at (a) 0°, (b) 45°, (c) 90°, and (d) 135°.

3. Diffraction from a Binary Polarization Grating

A PDG is a space-variant periodic polarization element. Unlike classical phase or amplitude diffraction gratings, they introduce a periodic change of the polarization state, thus leading to a polarization-dependent diffraction pattern. Therefore, PDG are effective tools for polarization measurements in polarimetry and ellipsometry applications [14]. Here we consider the simplest case, a binary PDG, which can be directly displayed in our previously characterized FLCoS display. We apply a theoretical analysis for these gratings based on the Jones–Fourier formalism developed in [18]. That method states that a spatially-dependent polarization mask is described by a Jones Matrix $\mathbf{M}(x)$, and its diffraction pattern can be calculated by a related Jones–Fourier matrix $\tilde{\mathbf{M}}(u)$, whose elements are the Fourier transform of the corresponding elements of $\mathbf{M}(x)$, with u being the spatial frequency. The diffraction pattern generated when the polarization mask is illuminated with a given polarization state is calculated by multiplying the Jones vector of the input beam (V_{in}) by the Jones–Fourier matrix $\tilde{\mathbf{M}}(u)$. The advantage of using the matrix $\tilde{\mathbf{M}}(u)$ is that it simultaneously accounts for the polarization transformation at the grating and the polarization transformation during the propagation, thus leading to specific equivalent polarization elements for the whole process.

In this work we apply this method to analyze the specific case of a binary PDG, which is defined as a periodic succession of two polarization elements described by their corresponding Jones matrices, $\mathbf{M}_a$ and $\mathbf{M}_b$. For simplicity we consider a grating with a 50% fill factor. Assuming that the grating is infinitely extended, it can be expressed as the following Jones matrix:

$$\mathbf{M}(x) = \mathbf{M}_a \cdot \left(\text{rect}\left(\frac{x}{p/2}\right) \otimes \sum_n \delta(x - np) \right) + \mathbf{M}_b \cdot \left(\text{rect}\left(\frac{x}{p/2}\right) \otimes \sum_n \delta(x - np - p/2) \right), \quad (2)$$

where n are integer numbers, p is the grating's period, $\otimes$ indicates the convolution operation, $\delta(\cdot)$ is the Dirac delta distribution, and rect$(\cdot)$ is the rectangle function defined as [19]

$$\mathrm{rect}(x) = \begin{cases} 1 & \text{if } |x| < 1/2 \\ 1/2 & \text{if } |x| = 1/2 \\ 0 & \text{if } |x| > 1/2 \end{cases}. \tag{3}$$

The Jones–Fourier matrix $\tilde{\mathbf{M}}(u)$, calculated by Fourier transforming each component of the Jones matrix in Eq. (2), results in

$$\tilde{\mathbf{M}}(u) = \frac{1}{2}(\mathbf{M}_a + \mathbf{M}_b \exp(-i\pi u p))\mathrm{sinc}\left(\frac{p}{2}u\right) \cdot \sum_n \delta\left(u - \frac{n}{p}\right), \tag{4}$$

where $\mathrm{sinc}(x) \equiv \sin(x\pi)/(x\pi)$ is the Fourier transform of the rectangle function. This equation can be rewritten as

$$\tilde{\mathbf{M}}(u) = \sum_n \tilde{\mathbf{M}}_n \cdot \delta\left(u - \frac{n}{p}\right), \tag{5}$$

where $\tilde{\mathbf{M}}_n$ are the Jones matrices characterizing the PDG action on the nth diffracted order. These matrices are given by

$$\tilde{\mathbf{M}}_n = \frac{1}{2}\mathrm{sinc}\left(\frac{n}{2}\right)(\mathbf{M}_a + \mathbf{M}_b \exp(-i\pi n)) = a_n(\mathbf{M}_a + \mathbf{M}_b \exp(-i\pi n)). \tag{6}$$

Note that the amplitude factors $a_n = (1/2)\cdot \mathrm{sinc}(n/2)$ are exactly the amplitude of the diffraction orders generated by a standard binary amplitude grating, with transmission levels 1 and 0 [20]. Equations (5) and (6) reveal that the polarization grating generates a set of diffraction orders located at spatial frequencies $u_n = n/p$ (like scalar amplitude or phase gratings), but each order has a vector field that is defined by the Jones matrix $\tilde{\mathbf{M}}_n$. Like in the case of a binary amplitude or phase grating with a 50% fill factor, all even diffraction orders are cancelled because the sinc function in Eq. (6) becomes null. The zero order ($n = 0$, DC term) is characterized by a Jones matrix resulting from adding the two matrices of the grating together, i.e.,

$$\tilde{\mathbf{M}}_{n=0} = \frac{\mathbf{M}_a + \mathbf{M}_b}{2}. \tag{7}$$

On the contrary, the odd diffraction orders are characterized by a Jones matrix defined in terms of the difference between the two Jones matrices of the grating; i.e.,

$$\tilde{\mathbf{M}}_{\mathrm{odd}\,n} = \pm\frac{\mathbf{M}_a - \mathbf{M}_b}{n\pi}. \tag{8}$$

If the polarization grating is illuminated with a polarization state described by a Jones vector V_{in}, the two states emerging from the display are $V_a = \mathbf{M}_a V_{\mathrm{in}}$ and $V_b = \mathbf{M}_b V_{\mathrm{in}}$, while the Jones vectors at the diffraction orders are given by $\tilde{V}_n = \tilde{\mathbf{M}}_n V_{\mathrm{in}}$. We note that results equivalent to those in Eqs. (7) and (8) were already derived in [6], using a different formalism based on the Poincaré sphere, which was applied there to analyze binary as well as continuous polarization gratings.

4. Half-Wave Plate Polarization Diffraction Grating

We start by considering the simplest case, where the two levels in the PDG correspond to an HWP with two different axes orientations with a relative angle of $\Delta\theta = 45°$. This type of grating can be addressed directly onto our LCoS display when we illuminate it with wavelength $\lambda = 568\,\mathrm{nm}$, since the phase shift is practically 180°. For simplicity, and although our device is a reflective display, we do not consider the polarization transformation that happens due to the reflection (we consider the equivalent transmissive display). Before discussing the experimental results, we summarize the theoretical analysis of such an HWP PDG.

A. Theoretical Analysis

The details on the application of the results in Section 3 to this type of polarization grating are presented in Appendix A, where we analyze the more general case for a binary PDG with arbitrary phase shift ϕ and arbitrary tilt angle $\Delta\theta$. The main result is that the action of such a general PDG and the subsequent propagation to the Fourier diffraction plane is equivalent, for the odd diffracted orders, to the action of an HWP oriented at $\Delta\theta/2$–45°, independent of the phase shift introduced by the FLC. Furthermore, for the specific case considered here, with $\phi = 180°$ and $\Delta\theta = 45°$, the PDG action is equivalent to that a of an HWP oriented at –22.5 for the odd diffraction orders, and to that of an HWP oriented at +22.5° for the DC order.

We consider, for simplicity, input linear polarization with arbitrary orientation α (the input Jones vector is $V_{\mathrm{in}} = (\cos(\alpha)\,\sin(\alpha))^t$, where the superindex t denotes the transposed matrix). As is demonstrated Appendix A, the Jones vectors characterizing the diffracted orders generated by this binary HWP PDG are given by

$$\tilde{V}_{n=0} = \frac{1}{\sqrt{2}}\begin{pmatrix} \cos(45° - \alpha) \\ \sin(45° - \alpha) \end{pmatrix}, \tag{9a}$$

$$\tilde{V}_{\mathrm{odd}\,n} = \pm\frac{\sqrt{2}}{n\pi}\begin{pmatrix} \cos(-45° - \alpha) \\ \sin(-45° - \alpha) \end{pmatrix}. \tag{9b}$$

Therefore, the polarization states of the DC and diffracted orders are linear and orthogonal (oriented at $45° - \alpha$ and $-45° - \alpha$, respectively). Moreover, this property is independent of the input polarization angle (α). The intensity of the diffracted orders is also independent of the input state of polarization and it is given by

$$i_n = \begin{cases} 1/2 & \text{for } n = 0 \\ \frac{2}{(n\pi)^2} & \text{for odd } n \\ 0 & \text{for even } n \neq 0 \end{cases}. \tag{10}$$

It is interesting to note that these intensity values exactly double those corresponding to an equivalent binary amplitude grating [20]. Particularly relevant is the intensity of the first ($n = 1$) diffraction order, since it defines the modulation diffraction efficiency (η). It describes the diffraction efficiency of a diffractive optical element addressed to the display [21]. For this particular case, a value $\eta = 20.3\%$ is obtained. Figure 4 shows the polarization states involved in these situations, including the input polarization, the two polarizations emerging from the display (V_a and V_b), and the two polarizations corresponding to the DC and the diffracted orders ($\tilde{V}_0$ and $\tilde{V}_n$). Figures 4(a) and 4(b) show, respectively, the states corresponding to illuminating the PDG with linear polarization oriented at $\alpha = 0$ (the standard configuration for display application) and with an arbitrary α.

The fact that the two emerging states are linear and orthogonal allows operating the display as a binary amplitude or as a binary phase grating by simply using an analyzer. This is indicated in Fig. 4(c), where the analyzer's orientation is drawn as a discontinuous arrow. In this figure we represent the

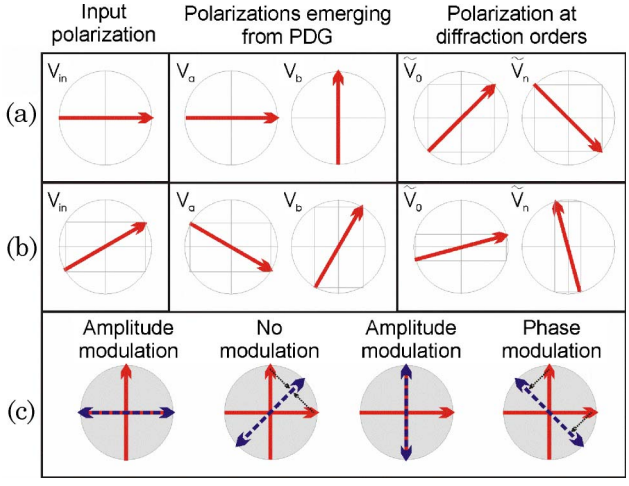

Fig. 4. (Color online) Polarization states involved in the ideal half-wave plate PDG. V_{in} is the incident polarization. V_a and V_b are the two states emerging from the PDG. $\tilde{V}_0$ and $\tilde{V}_n$ are the states at the DC and at the odd diffracted orders. (a) $\alpha = 0°$. (b) α is arbitrary. (c) Analyzer orientation (discontinuous blue arrow), relative to the two states emerging from the PDG, to obtain amplitude modulation, phase modulation, or absence of modulation.

two emerging states in the vertical and the horizontal direction. When the analyzer is parallel to one of the two emerging states (and is therefore crossed to the other emerging state) this state is fully transmitted, while the other one is fully absorbed. The result is a binary amplitude grating, with amplitude transmissions of 100% and zero in each region. On the contrary, binary π phase modulation is achieved by orienting the analyzer perpendicular to the line that bisects the two emerging states [22]. This π phase is generated by the opposite projection sense of the two linear states onto the analyzer orientation. Note that in this situation the analyzer is perpendicular to the linear polarization state in the DC order, which is therefore cancelled (as it corresponds for a binary phase grating with π phase shift). On the contrary, when the analyzer bisects the two states emerging from the PDG, the projection of these states onto the analyzer occurs with the same sign, and no phase modulation is produced. In this case, the analyzer orientation is crossed to the orientation of all diffracted orders, which therefore vanish, in agreement with the absence of modulation.

To compare the different configurations described above, it is useful to calculate the diffraction efficiency of the gratings, η. This can be evaluated within the Jones formalism, by multiplying the Jones matrix of the analyzer (with orientation θ_{P2}) by the Jones vector of Eq. (9b), and calculating the intensity for the $n = 1$ order. The diffraction efficiency of the four gratings shown in Fig. 4 is more easily calculated if we consider an incident linear polarization state ($\alpha = 0°$) and hence take $\theta_{P2} = 0°$, 45°, 90°, and 135°. The resulting modulation efficiencies are, respectively, $\eta = 10.1\%$, 0%, 10.1%, and 20.3%. For the amplitude modulation configurations ($\theta_{P2} = 0°$ and 90°), the efficiency is equal to that of an amplitude grating, while for the phase modulation configuration ($\theta_{P2} = 135°$) it is half of that of a perfect phase-only grating, since the analyzer absorbs half of the total intensity (that in the DC order). These values, however, represent the absolute diffraction efficiency. To better evaluate the PDG performance as amplitude or phase gratings, we define a relative diffraction efficiency (η_{rel}) as the ratio of the first diffraction order intensity with respect to the total intensity behind the analyzer. The values of η_{rel} corresponding to $\theta_{P2} = 0°$, 45°, 90°, and 135° are, respectively, $\eta_{\text{rel}} = 20.3\%$, 0%, 20.3%, and 40.6%, where the latter shows the perfect binary π-phase modulation regime. This discussion illustrates how binary amplitude and phase gratings can be regarded as specific cases of the more general binary PDG.

B. Experimental Realization and Configurations for Scalar Gratings

The experimental realization of such an ideal HWP PDG can be done in our FLCoS display by illuminating it with wavelength $\lambda = 568$ nm, which provides a phase shift of almost $\phi = 180°$. We modified the

experimental setup in Fig. 1(a) by inserting a spatial filter and a converging lens to illuminate the display with a collimated beam. A second converging lens is included in the reflected beam, so the Fourier diffraction can be captured by placing a CCD camera in its back focal plane. A binary grating with gray levels 255 (white) and 0 (black), a period of 16 pixels, and a 50% fill factor (8 pixels black and 8 pixels white) is addressed to the display. Figure 5(a) shows the diffraction pattern when no analyzer is placed on the reflected beam. The input polarizer is oriented at $\theta_1 = 0°$, i.e., parallel to the first LC position (thus reproducing the scheme represented in Fig. 4(a)]. The diffraction pattern shows the diffraction orders characteristic of a binary grating: the central (DC) order is the strongest, and the even diffraction orders are absent. However, the polarization state of the DC order is orthogonal to that of the odd diffracted orders, as it can be shown by placing an analyzer on the reflected beam.

Figures 5(b)–5(e) show the diffraction pattern when the analyzer is included, with the same orientations as we used in Fig. 3 (i.e, the analyzer is oriented at $\theta_{P2} = 0°$, 45°, 90°, and 135°, respectively). In Figs. 5(b) and 5(d) the analyzer is oriented parallel to one of the two states emerging from the grating, thus bisecting the polarizations state on the diffraction orders. These two orientations reproduce the binary amplitude diffraction grating, and the pattern looks like that without analyzer. However, when the analyzer is oriented at 45° [Fig. 5(c)], it bisects the two states emerging from the grating, and it coincides with the polarization orientation at the DC order. This orientation is orthogonal to the polarization of the diffracted orders, which are cancelled, and no diffraction grating effect appears in this case. Finally, Fig. 5(e) shows the pattern when the analyzer is oriented at 135°. Now the DC order disappears, and the diffracted orders are enhanced. This case corresponds to a binary π phase grating. Let us note that we can thus easily identify the phase modulation configuration in the experiment shown in Fig. 3, when the intensity shows narrow peaks pointing down [Fig. 3(d)].

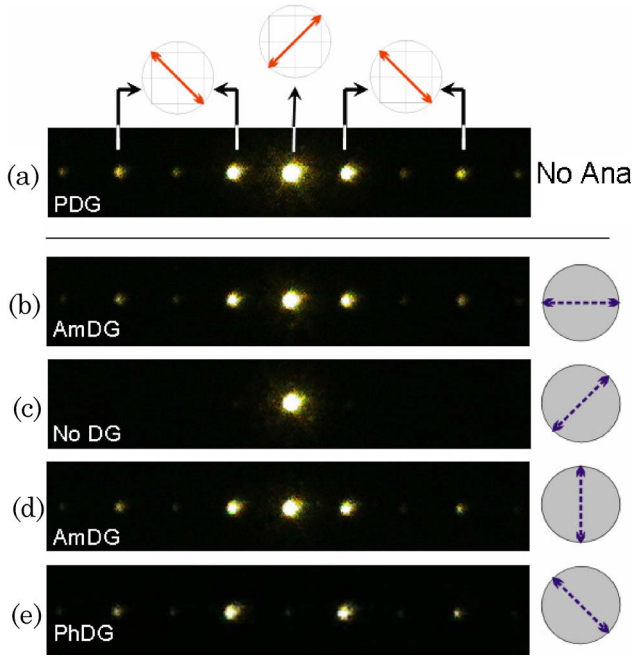

Fig. 5. (Color online) Experimental diffraction pattern of the binary HWP–PDG obtained for $\lambda = 568$ nm. Input polarizer is oriented at $\theta_{P1} = 0°$. (a) Case without analyzer. (b)–(e) Cases with the analyzer oriented at (b) $\theta_{P2} = 0°$, (c) $\theta_{P2} = 45°$, (d) $\theta_{P2} = 90°$, and (e) $\theta_{P2} = 135°$. PDG, AmDG, and PhDG indicate the configurations for polarization, amplitude, and phase diffraction grating. No DG indicates the configuration for the absence of grating.

C. Simplified Configuration with a Single Polarizer

The result in Eqs. (9) can be used to simplify the setup, by using one single polarizer acting both on the input and the reflected beams. For that purpose, the polarizer is placed close to the FLCoS display. Now the analyzer is fixed to be at the same orientation as the input polarization. However, this is not a limitation to obtain configurations for amplitude and phase binary gratings, although the suitable angles change and they must be properly selected. Table 1 summarizes the orientation of the linear states for the input beam, of the two states (a and b) emerging from the display, and of the DC and diffracted odd orders. θ_P represents the angle of the input linear polarization (and therefore also the orientation transmitted by the analyzer). Now, for $\theta_P = 0°$ and for $\theta_P = 45°$ the analyzer coincides with one of the states emerging from the grating (a and b), and therefore amplitude modulation is obtained. On the contrary, for $\theta_P = 22.5°$, the configuration corresponds to the absence of modulation (only the DC order is transmitted), while the π-phase modulation configuration is obtained for $\theta_P = 67.5°$, where only the diffracted odd orders are transmitted by the analyzer.

The corresponding experimental diffraction patterns, captured as the polarizer was rotated in steps of 22.5°, are presented in Fig. 6. Figures 6(a) and 6(c) show the patterns when the polarizer is oriented at $\theta_P = 0°$ and 45°, respectively, and presents the characteristics of the amplitude gratings (the DC order is stronger than the diffracted orders). For $\theta_P = 22.5°$ only the DC order is present, thus providing the situation without modulation. Finally, for $\theta_P = 67.5°$ the DC order is cancelled and only the odd diffracted orders are present, denoting the π-phase grating. These results prove that binary amplitude and binary phase regimes can be accomplished with a

Table 1. Angular Orientation of the Linear Polarization States Involved in the HWP PDG

Input	State a	State b	DC Order	Odd Orders
θ_P	$-\theta_P$	$90 - \theta_P$	$45 - \theta_P$	$-45 - \theta_P$
0	0	90	45	−45
22.5	−22.5	67.5	22.5	−67.5
45	−45	45	0	−90
67.5	−67.5	22.5	−22.5	67.5

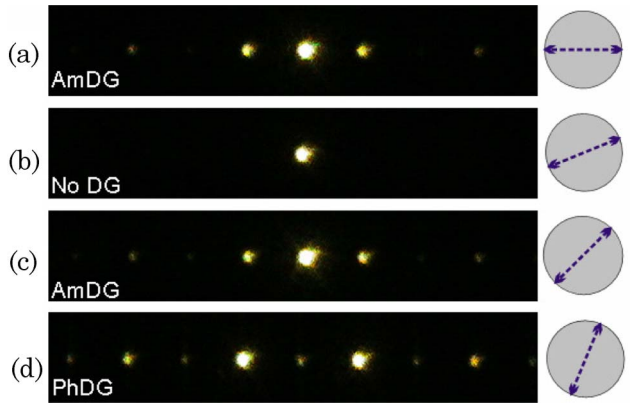

Fig. 6. (Color online) Experimental diffraction pattern of the binary grating obtained for the wavelength $\lambda = 568$ nm. Configuration with a single polarizer oriented at (a) $\theta_P = 0°$, (b) $\theta_P = 22.5°$, (c) $\theta_P = 45°$, and (d) $\theta_P = 67.5°$.

single polarizer, thus simplifying the experimental configuration.

5. Arbitrary Phase-Shift Polarization Diffraction Grating

This final section deals with PDG when phase shift ϕ, introduced by the LC layer, differs from the ideal value of 180°. As was demonstrated in Section 2, this occurs when the operating wavelength is different from the design one [23]. In this situation, the states emerging from the display are, in general, elliptically polarized and not orthogonal. We recently analyzed this situation and how it leads to a reduction in the contrast ratio in display applications. We proposed a method to compensate this effect by introducing a QWP before the modulator to illuminate the display with the proper polarization that yields, at the output, two states with the maximum degree of orthogonality [12,13].

In the application for diffraction gratings, the effect of the phase mismatch is a reduction in the diffraction efficiency. Here we make a further step in the technique proposed in [12] to compensate for this PDG diffraction efficiency loss. The diffraction efficiency can be evaluated from the discussion in Appendix A [Eqs. (A8)–(A11)]. We evaluate efficiency loss with a parameter r defined as the ratio between the total diffracted intensity (i.e., the parameter η_D defined in Eq. (A10) of the Appendix, equal to the sum of the intensity of all the odd diffracted orders) generated with the nonideal PDG ($\Delta\theta = 45°$ and arbitrary ϕ) and the corresponding value for the ideal case ($\Delta\theta = 45°$ and $\phi = 180°$). From Eq. (A10) it is direct to obtain that

$$r = \sin^2\left(\frac{\phi}{2}\right). \tag{11}$$

For instance, let us analyze the standard configuration, where the display is illuminated with linearly polarized light oriented at $\theta_{P1} = 0°$, and the phase shift is $\phi = 105°$ (which corresponds to

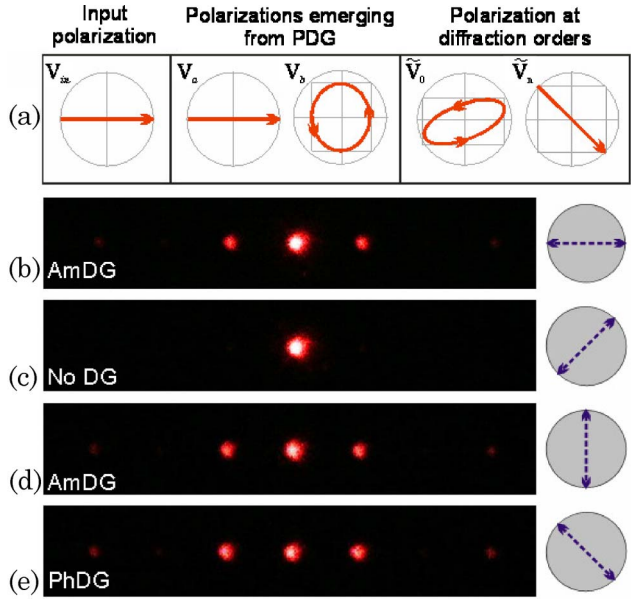

Fig. 7. (Color online) (a) Polarization states involved in a nonideal PDG ($\phi \neq 180°$, $\Delta\theta = 45°$). The input polarizer is oriented at $\theta_{P1} = 0°$. (b)–(e) Experimental diffraction patterns obtained for $\lambda = 647$ nm with different orientations of the analyzer ($\theta_{P2} = 0°$, 45°, 90°, and 135°), which is indicated on the right.

illumination with the red laser line, $\lambda = 647$ nm). The odd diffracted orders always remain linearly polarized at −45°, independent of the value of ϕ, but their intensity has been reduced by a factor $r = 0.63$ for $\phi = 105°$ in comparison with the intensity obtained in the ideal case ($\phi = 180°$). This means that, without analyzer, the modulation diffraction efficiency is now reduced to 12.8% (the value in the ideal case was 20.3%). For the amplitude and phase configurations, the efficiency is now reduced to $\eta = 6.4\%$ and 12.8%, respectively (the values in the ideal configuration were 10.1% and 20.3%, respectively). On the contrary, the DC zero order is elliptically polarized, being the ellipse dependent on ϕ. Figure 7(a) shows the specific polarization ellipses for $\phi = 105°$, and Table 2 give the corresponding azimuth and ellipticity angles following the sign convention in [13]. While one of the two states emerging from the PDG remains linearly polarized (V_a), the second state (V_b) becomes elliptically polarized. Figure 7(a) also indicates the polarization states corresponding to the DC and diffracted orders ($\tilde{V}_0$ and $\tilde{V}_n$, respectively), which show that the DC order is now elliptically polarized. This means that the intensity of the DC order cannot be cancelled with the analyzer, or equivalently, binary phase-only modulation cannot be accomplished. Figures 7(b)–7(e) present the

Table 2. Elliptical States Involved in the Standard Configuration Corresponding to Fig. 7 ($\phi = 105°$)

	Input	State a	State b	DC Order	Odd Orders
Azimuth (α)	0°	0°	90°	20.1°	135°
Ellipticity (ϵ)	0°	0°	37.5°	22.4°	0°

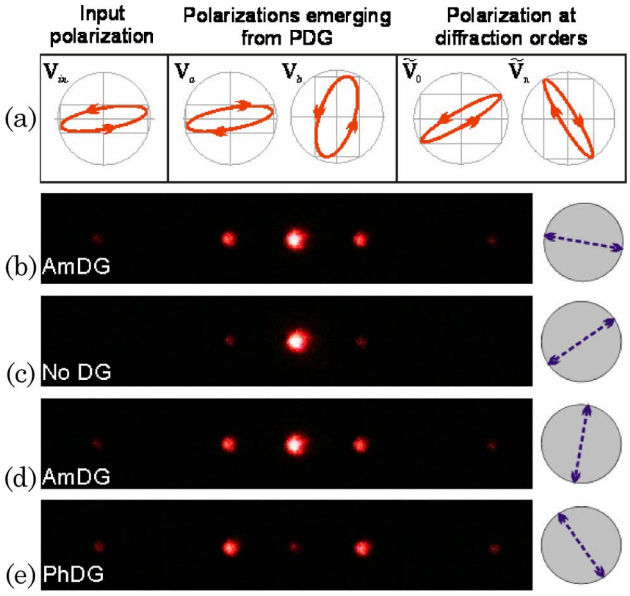

Fig. 8. (Color online) (a) Polarization states involved in a compensated nonideal PDG ($\phi \neq 180°$, $\Delta\theta = 45°$). (b)–(e) Experimental diffraction patterns obtained for $\lambda = 647\,\text{nm}$ with different orientations of the analyzer ($\theta_{P2} = -12°$, 33°, 78°, and 123°), which is indicated on the right.

experimental diffraction patterns captured in the same configurations as those in Figs. 5(b)–5(e). The results for the amplitude configurations [Figs. 7(b) and 7(d)] look similar to those in the ideal case [Figs. 5(b) and 5(d)], although the diffraction efficiency has been reduced. The case without modulation [Fig. 7(c)] is also equivalent to the ideal case [Fig. 5(c)]: all diffracted orders are cancelled in this configuration since the analyzer is crossed to their linear polarization. The diffraction efficiency reduction is clearly visible in the phase modulation configuration [Fig. 7(e)], which notably differs from the ideal case [Fig. 5(e)] in the presence of a strong DC peak. This is also clear in the evaluation of the relative efficiency, which now is reduced to a value $\eta_{\text{rel}} = 25.5\%$ (for the ideal case it was $\eta_{\text{rel}} = 40.6\%$). The situation is equivalent to having a binary phase modulation, but with a phase shift different from the ideal value of 180° [24].

This drawback can be overcome by following the procedure we introduced in [12] and analyzed extensively in [13], where a QWP is inserted between the input polarizer and the FLC display to generate the proper incident elliptical polarization that provides

Table 3. Elliptical States Involved in the Optimized Configuration Corresponding to Fig. 8

	Input	State a	State b	DC Order	Odd Orders
Azimuth (α)	10.6°	8.4°	74.8°	33.1°	124.4°
Ellipticity (ϵ)	10.6°	−12.4°	24.1°	11.9°	−10.6°

two states as close as possible that are linear and orthogonal. The difference in our approach here is that we apply this procedure to make the two polarization states of the DC and odd diffraction orders linear and orthogonal (whereas in our previous papers the goal was to have these characteristics for the two emerging states of the FLC to enhance the contrast ratio). The fact that the polarization states on the diffracted orders become linear and orthogonal makes it possible to obtain amplitude or phase modulation configurations by simply rotating the analyzer, in the same manner as was discussed previously in the ideal case.

Following the procedure described in [12,13], we have calculated the orientations of the input polarizer and the QWP. They depend on phase shift ϕ. For the value $\phi = 105°$, the best results are obtained when the first polarizer is oriented at $\theta_{P1} = 0°$ and the QWP is oriented at 10.6°. Figure 8(a) shows the polarization ellipses involved in this configuration, and Table 3 gives the corresponding azimuth and ellipticity angles. Now the input beam and the two states emerging from the display are all elliptically polarized. However, in the diffraction pattern, the states corresponding to the DC and the odd diffracted orders show low and opposite signed ellipticity and nearly orthogonal azimuths, oriented at 33° and 124°, respectively. Figures 8(b)–8(e) show the experimental diffraction patterns for $\lambda = 647\,\text{nm}$ and for this optimized configuration as we rotate the analyzer (now θ_{P2} is oriented at angles −12°, 33°, 78°, and 123°, respectively). The absolute diffraction efficiency at these configurations are, respectively, $\eta =$ 6.7%, 0.4%, 6.1%, and 12.3%. These values do not show an improvement with respect to those in the previous configuration. However, the relative efficiency is clearly improved for the phase modulation configuration, reaching a value $\eta_{\text{rel}} = 37.0\%$. This result is comparable to that obtained in the ideal case (Fig. 5), becoming especially clear in the almost perfect absence of the DC order [Fig. 8(e)]. Therefore the device phase-shift mismatch has been compensated and the ideal modulation response is almost

Table 4. Absolute (η) and Relative (η_{rel}) Diffraction Efficiencies for the Considered Binary PDG Configurations[a]

Grating Configuration	Ideal HWP PDG (Fig. 5) (%)	Nonideal PDG (Fig. 7) (%)	Compensated Nonideal PDG (Fig. 8) (%)
No Analyzer	$\eta = 20.3$	$\eta = 12.8$	$\eta = 12.8$
AmDG1	$\eta = 10.1$ $\eta_{\text{rel}} = 20.3$	$\eta = 6.4$ $\eta_{\text{rel}} = 9.3$	$\eta = 6.7$ $\eta_{\text{rel}} = 13.2$
NoDG	$\eta = 0.0$ $\eta_{\text{rel}} = 0.0$	$\eta = 0.0$ $\eta_{\text{rel}} = 0.0$	$\eta = 0.4$ $\eta_{\text{rel}} = 0.7$
AmDG2	$\eta = 10.1$ $\eta_{\text{rel}} = 20.3$	$\eta = 6.4$ $\eta_{\text{rel}} = 20.2$	$\eta = 6.1$ $\eta_{\text{rel}} = 12.3$
PhDG	$\eta = 20.3$ $\eta = 40.6$	$\eta = 12.8$ $\eta_{\text{rel}} = 25.5$	$\eta = 12.3$ $\eta_{\text{rel}} = 37.0$

[a]AmDG, NoDG, and PhDG denote the configurations for amplitude, absence, and phase grating, respectively.

perfectly recovered. The values of the calculated absolute and relative diffraction efficiencies of this and previous configurations are summarized in Table 4.

6. Conclusions

In summary, we have presented a complete study on binary PDG displayed on a FLCoS display. We first applied a reverse engineering technique to characterize the physical parameters of our display. Then we applied the Jones–Fourier formalism to analyze a binary PDG with switching angle $\Delta\theta = 45°$ and arbitrary phase shift ϕ and revealed that the action of such PDG can be regarded as that of an HWP oriented at $-22.5°$ for the odd diffracted orders, regardless of the value of ϕ. In addition, when the phase shift is $\phi = 180°$, the action on the DC order is equivalent to that of an HWP oriented at $+22.5°$. Based on this polarization analysis, we showed how this PDG can be converted onto amplitude or phase gratings by properly projecting the polarization states onto an analyzer. As a result of this analysis, we presented two improvements. The first one is a simplification of the system using a single polarizer for both the input and reflected beams, which provides equivalent results for amplitude or phase modulation as the operational mode involving two polarizers. Secondly, we analyzed the PDG performance when the phase shift differs from the ideal value (typically because of wavelength dispersion). We showed that the ideal performance can be almost perfectly recovered by illuminating the display with the proper elliptical polarization. For instance an almost perfect π phase shift, phase-only diffraction grating has been demonstrated with a wavelength providing a phase shift far from the ideal value $\phi = 180°$, simply with a reduction in diffraction efficiency.

All the theoretical results have been experimentally demonstrated by employing two laser lines with different wavelengths: one (568 nm) giving almost perfect HWP behavior, while the second one (647 nm) shows an important phase-shift mismatch. This study is, therefore, a useful guide to correctly operate a FLCoS display for polarization, amplitude, or phase modulation regimes, which is interesting for programmable diffractive optics applications.

Appendix

Here we include the derivations of the expressions of the Jones vectors and matrices related to the diffraction orders generated by the binary polarization gratings discussed in this paper. We consider a generic case with an arbitrary phase shift ϕ and arbitrary switching angle $\Delta\theta$. For simplicity, we assume the two LC stable angular orientations (a and b) are located at $0°$ and θ, respectively (i.e., $\Delta\theta = \theta$). The Jones matrices describing these two states are, respectively, [25]

$$\mathbf{M}_a = \mathbf{M}_{WP}(\phi, \theta = 0°) = \begin{pmatrix} 1 & 0 \\ 0 & e^{i\phi} \end{pmatrix}, \tag{A1}$$

$$\begin{aligned} \mathbf{M}_b &= \mathbf{M}_{WP}(\phi, \theta) = \mathbf{R}(-\theta)\mathbf{M}_{WP}(\phi°, \theta = 0°)\mathbf{R}(\theta) \\ &= \begin{pmatrix} \cos^2(\theta) + \sin^2(\theta)e^{i\phi} & \sin(\theta)\cos(\theta)(1 - e^{i\phi}) \\ \sin(\theta)\cos(\theta)(1 - e^{i\phi}) & \sin^2(\theta) + \cos^2(\theta)e^{i\phi} \end{pmatrix}, \end{aligned} \tag{A2}$$

where $\mathbf{M}_{WP}(\phi, \theta)$ denotes the Jones matrix for a wave plate with phase shift ϕ and orientation θ, and where $\mathbf{R}(\theta)$ is the rotation 2×2 matrix:

$$\mathbf{R}(\theta) = \begin{pmatrix} \cos(\theta) & \sin(\theta) \\ -\sin(\theta) & \cos(\theta) \end{pmatrix}. \tag{A3}$$

Thus, the Jones–Fourier matrices corresponding to the DC and odd diffracted orders are given by Eqs. (7) and (8), and they can be written as

$$\tilde{\mathbf{M}}_{n=0} = \frac{1}{2}\begin{pmatrix} 1 + \cos^2(\theta) + \sin^2(\theta)e^{i\phi} & \sin(\theta)\cos(\theta)(1 - e^{i\phi}) \\ \sin(\theta)\cos(\theta)(1 - e^{i\phi}) & \sin^2(\theta) + [1 + \cos^2(\theta)]e^{i\phi} \end{pmatrix}, \tag{A4}$$

$$\tilde{\mathbf{M}}_{\text{odd}\,n} = \pm\frac{\sin(\theta)(1 - e^{i\phi})}{n\pi}\begin{pmatrix} \sin(\theta) & -\cos\theta \\ -\cos(\theta) & -\sin(\theta) \end{pmatrix}. \tag{A5}$$

Let us note that the Jones matrix corresponding to an HWP rotated by an angle θ' is equal to

$$\begin{aligned} \mathbf{M}_{WP}(\phi = 180°, \theta') &= \mathbf{R}(-\theta')\mathbf{M}_{WP}(\phi = 180°, \theta' = 0°)\mathbf{R}(\theta') \\ &= \begin{pmatrix} \cos(2\theta') & \sin(2\theta') \\ \sin(2\theta') & -\cos(2\theta') \end{pmatrix}. \end{aligned} \tag{A6}$$

Therefore, Eq. (A5) can be rewritten as

$$\begin{aligned} \tilde{\mathbf{M}}_{\text{odd}\,n} &= \pm\frac{\sin(\theta)(1 - e^{i\phi})}{n\pi} \\ &\times \mathbf{M}_{WP}\left(\phi = 180°, \theta' = \frac{\theta}{2} - 45°\right). \end{aligned} \tag{A7}$$

This is a relevant result since it reveals that the action of the PDG and the subsequent propagation

to the Fourier diffraction plane is equivalent, for the odd diffraction orders, to the action of an HWP oriented at $\theta' = \theta/2 - 45°$, independent of phase shift ϕ introduced by the FLCD. Therefore, if the polarization of the beam incident on the PDG is linear with orientation α, the typical action of the HWP will provide, at the odd diffraction orders, linear polarization with orientation $\theta - \alpha - 90°$, independent of the value of ϕ. On the contrary, according to Eq. (A4), the DC term will present in general elliptical polarization.

Since the matrix $\mathbf{M}_{WP}$ in Eqs. (A7) does not change the light power, the intensity (i_n) of the odd diffracted orders is directly given by the square modulus of the amplitude term in front of the matrix, i.e.,

$$i_{\text{odd}\,n} = \frac{4}{n^2\pi^2}\sin^2(\theta)\sin^2\left(\frac{\phi}{2}\right), \tag{A8}$$

while the intensity of all even orders is always zero. In particular, the modulation diffraction efficiency (η) is the intensity of the $n = 1$ order, i.e.,

$$\eta = i_{n=1} = \frac{4}{\pi^2}\sin^2(\theta)\sin^2\left(\frac{\phi}{2}\right). \tag{A9}$$

The total diffracted intensity η_D (the addition of the intensities of all diffracted orders except the zero order) can be calculated by

$$\eta_D = \sum_{n\neq 0} i_n = \frac{8}{\pi^2}\sin^2(\theta)\sin^2\left(\frac{\phi}{2}\right)$$
$$\sum_{n=1,3,5\ldots}\frac{1}{n^2} = \sin^2(\theta)\sin^2\left(\frac{\phi}{2}\right), \tag{A10}$$

where we assumed that orders $\pm n$ have equal intensities, and that the summation in this equation equals $\pi^2/8$. Therefore, the intensity of the undiffracted zero order (DC term) is given by

$$i_0 = 1 - \eta_D = 1 - \sin^2(\theta)\sin^2\left(\frac{\phi}{2}\right)$$
$$= \cos^2(\theta) + \frac{1}{2}\sin^2(\theta)(1+\cos\phi). \tag{A11}$$

Therefore, Eqs. (A8) and (A11) provide the intensities of the diffracted orders in terms of phase shift ϕ and switching angle θ. It is important to remark that these intensities are independent of the input beam polarization state. We also want to remark that these expressions for the intensities of the diffracted orders can be directly derived in a different manner using the formulation in [7].

Finally, we apply the above expressions to the specific values of phase shift and switching angle of our device. If $\theta = 45°$, the equivalent Jones matrix for odd diffracted orders becomes an HWP oriented at $-22.5°$. If, in addition, the phase shift is $\phi = 180°$, the Jones matrices describing the DC and diffracted orders [Eqs. (A4) and (A5)] become

$$\tilde{\mathbf{M}}_{n=0} = \frac{1}{2}\begin{pmatrix} +1 & +1 \\ +1 & -1 \end{pmatrix}$$
$$= \frac{1}{\sqrt{2}}\mathbf{M}_{WP}(\phi = 180°, \theta = +22.5°), \tag{A12}$$

$$\tilde{\mathbf{M}}_{\text{odd}\,n} = \pm\frac{1}{n\pi}\begin{pmatrix} +1 & -1 \\ -1 & -1 \end{pmatrix}$$
$$= \pm\frac{\sqrt{2}}{n\pi}\mathbf{M}_{WP}(\phi = 180°, \theta = -22.5°). \tag{A13}$$

In this case the Jones matrix corresponding to the DC order also represents an HWP but is oriented at $+22.5°$. If we consider an arbitrary input linear polarization, with orientation α, the input Jones vector is $V_{\text{in}} = (\cos(\alpha)\,\sin(\alpha))^t$ (with superindex t meaning the transposed matrix), and by means of Eqs. (A1) and (A2) the two polarizations emerging from the PDG are given by

$$V_a = \mathbf{M}_a \cdot \begin{pmatrix} \cos(\alpha) \\ \sin(\alpha) \end{pmatrix} = \begin{pmatrix} \cos(-\alpha) \\ \sin(-\alpha) \end{pmatrix}, \tag{14}$$

$$V_b = \mathbf{M}_b \cdot \begin{pmatrix} \cos(\alpha) \\ \sin(\alpha) \end{pmatrix} = \begin{pmatrix} \cos(90 - \alpha) \\ \sin(90 - \alpha) \end{pmatrix}, \tag{A15}$$

i.e., they are two linear and orthogonal states oriented at $-\alpha$ and $90° - \alpha$, respectively. The Jones vectors characterizing the diffracted orders generated with this binary PDG can be calculated using Eqs. (A12) and (A13), yielding

$$\tilde{V}_{n=0} = \tilde{\mathbf{M}}_{n=0} \cdot \begin{pmatrix} \cos(\alpha) \\ \sin(\alpha) \end{pmatrix} = \frac{1}{\sqrt{2}}\begin{pmatrix} \cos(45° - \alpha) \\ \sin(45° - \alpha) \end{pmatrix}, \tag{A16}$$

$$\tilde{V}_{\text{odd}\,n} = \tilde{\mathbf{M}}_{\text{odd}\,n} \cdot \begin{pmatrix} \cos(\alpha) \\ \sin(\alpha) \end{pmatrix} = \pm\frac{\sqrt{2}}{n\pi}\begin{pmatrix} \cos(-45° - \alpha) \\ \sin(-45° - \alpha) \end{pmatrix}. \tag{A17}$$

This result proves Eqs. (9) in this paper. The intensities in Eq. (10) are directly obtained from Eqs. (A8) and (A11) for $\theta = 45°$ and $\phi = 180°$.

This work was supported by Fondo Europeo de Desarrollo Regional (FEDER) funds and the Ministerio de Educación y Cultura of Spain (projects FIS2006-13037-C02-02 and FIS2007-60626).

References

1. J. L. Bougrenet de la Tocnaye and L. Dupont, "Complex amplitude modulation by use of a liquid crystal spatial light modulators," Appl. Opt. **36**, 1730–1741 (1997).

2. W. Osten, C. Kohler, and J. Liesener, "Evaluation and application of spatial light modulators for optical metrology," Opt. Pura Apl. **38**, 71–81 (2005).
3. J. Gourlay, S. Samus, P. McOwan, D. G. Vass, I. Underwood, and M. Worboys, "Real-time binary phase holograms on a reflective ferroelectric liquid-crystal spatial light modulator," Appl. Opt. **33**, 8251–8254 (1994).
4. I. G. Manolis, T. D. Wilkinson, M. M. Redmond, and W. A. Crossland, "Reconfigurable multilevel phase holograms for optical switches," IEEE Photon. Technol. Lett. **14**, 801–803 (2002).
5. M. Johansson, S. Hard, B. Robertson, L. Manolis, T. Wilkinson, and W. Crossland, "Adaptive beam steering implemented in a ferroelectric liquid-crystal spatial-light-modulator free-space, fiber-optic switch," Appl. Opt. **41**, 4904–4911 (2002).
6. P. Pellat-Finet, and M. Le Doucen, "Polarization properties of birefringence gratings," Optik (Jena) **100**, 159–166 (1995).
7. S. T. Warr and R. J. Mears, "Polarisation insensitive operation of ferroelectric liquid crystal devices," Electron. Lett. **31**, 714–716 (1995).
8. M. Le Doucen and P. Pellat-Finet, "Polarization properties and diffraction efficiencies of binary anisotropic gratings: general study and experiments on ferroelectric liquid crystals," Opt. Commun. **151**, 321–330 (1998).
9. W. J. Hossack, E. Theofanidou, J. Crain, K. Heggarty, and M. Birch, "High-speed holographic optical tweezers using a ferroelectric liquid crystal microdisplay," Opt. Express **11**, 2053–2059 (2003).
10. K. Heggarty, B. Fracasso, C. Letort, J. L. de Bougrenet de la Tocnaye, M. Brich, and D. Krüerke, "Silicon blackplane ferroelectric liquid crystal spatial light modulator for uses within an optical telecommunications environment," Ferroelectrics **312**, 39–55 (2004).
11. A. Martínez-García, I. Moreno, and M. M. Sánchez-López, "Comparative analysis of time and spatial multiplexed diffractive optical elements in a ferroelectric liquid crystal display," Jap. J. Appl. Phys. **47**, 1589–1594 (2008).
12. A. Martínez, N. Beaudoin, I. Moreno, M. M. Sánchez-López, and P. Velásquez, "Characterization and optimization of the constrast-ratio of a ferrroelectric liquid crystal optical modulator," J. Opt. A: Pure Appl. Opt. **8**, 1013–1018 (2006).
13. M. M. Sánchez-López, P. García-Martínez, A. Martínez-García, and I. Moreno, "Poincaré sphere analysis of a ferroelectric liquid crystal optical modulator: application to optimize the contrast ratio," J. Opt. A: Pure Appl. Opt. **11**, 015507 (2009).
14. G. Cincotti, "Polarization gratings: design and applications," IEEE J. Quant. Electron. **39**, 1645–1652 (2003).
15. F. Gori, "Measuring Stokes parameters by means of a polarization grating," Opt. Lett. **24**, 584–586 (1999).
16. J. Tervo and J. Turunen, "Paraxial-domain diffractive elements with 100% efficiency based on polarization gratings," Opt. Lett. **25**, 785–786 (2000).
17. J. A. Davis and G. H. Evans, "Polarizing binary diffraction grating beam splitter," Opt. Lett. **29**, 1443–1445 (2004).
18. I. Moreno, M. J. Yzuel, J. Campos, and A. Vargas, "Jones Matrix approach for polarization Fourier optics," J. Mod. Opt. **51**, 2031–2038 (2004).
19. J. W. Goodman, *Introduction to Fourier Optics* (McGraw-Hill, 1996).
20. A. Martínez, M. M. Sánchez-López, and I. Moreno, "Phasor analysis of binary amplitude gratings with different fill factor," Eur. J. Phys. **28**, 805–816 (2007).
21. I. Moreno, C. Iemmi, A. Márquez, J. Campos, and M. J. Yzuel, "Modulation light efficiency of diffractive lenses displayed in a restricted phase-mostly modulation display," Appl. Opt. **43**, 6278–6284 (2004).
22. J. A. Davis and M. A. Waring, "Contrast ratio improvement for the two-dimensional magneto-optic spatial light modulator," Appl. Opt. **31**, 6183–6184 (1992).
23. J. E. Stockley, G. D. Sharp, D. Doroski, and K. M. Johnson, "High-speed analog achromatic intensity modulator," Opt. Lett. **19**, 758–760 (1994).
24. J. L. Martinez, A. Martinez-Garcia, and I. Moreno, "Wavelength-compensated color Fourier diffractive optical elements using a ferroelectric liquid crystal on silicon display and a color-filter wheel," Appl. Opt. **48**, 911–918 (2009).
25. S. Huard, *Polarization of Light* (Wiley, 1997).